Effect of Material Attenuation on Lamb Wave Propagation in a Solar Cell Array

MATTIE GREEN, FADHEL ALSAFFAR, AJIT MAL
and CHRISTOPH SCHAAL

ABSTRACT

Satellites and other spacecraft rely on solar arrays for power. However, solar arrays are prone to a number of defects which are necessary to detect and repair. For example, bond line defects such as voids in the adhesive may be created during assembly, and disbonds may be caused by a mismatch in the coefficients of thermal expansion and cyclic thermal conditions in space. Lamb waves are a type of ultrasonic guided wave that have been used for nondestructive defect detection in laminates. In this work, they are used to evaluate disbonds at the adhesive interface. One feature of these waves that can be used for detecting and characterizing defects is the peak amplitude. However, material damping may have a significant effect on the amplitude of propagating Lamb waves, especially in polymeric materials. In this study, a single solar cell is modeled using a thermoplastic polymer for the substrate of the array, polycrystalline silicon for the solar cell, and a silicone-based adhesive. The material properties of the substrate, including material damping, are experimentally determined. Then transient structural finite element analyses are conducted on a 2 D model of a solar cell laminate with and without material damping effects included. The results of this study are intended to inform future in-space experiment design, but can also be applied to other layered media containing polymeric materials.

INTRODUCTION

Solar arrays are critical components of spacecraft as they provide power. The individual cells are made of silicon, a brittle crystalline material, and are bonded to a larger substrate. They are also electrically interconnected, so failure in one cell can disproportionately affect the efficiency of the entire array. Considering these factors, there has been significant work aimed towards the detection of microcracks in silicon wafers [1,2]. However, for in-space applications, cyclic thermal loads could also lead to bond line damage in a solar cell assembly. This is of particular interest where the substrate and

Mattie Green, Fadhel Alsaffar, Ajit Mal, Department of Mechanical and Aerospace Engineering, University of California, Los Angeles, CA, USA. Corresponding author: mattiegreen@g.ucla.edu. Christoph Schaal, Department of Mechanical and Aerospace Engineering, California State University, Northridge, CA, USA

cell have different coefficients of thermal expansion.

Lamb waves are ultrasonic guided waves that propagate parallel to the surface of thin plates. They are commonly used for defect detection in nondestructive evaluation (NDE) of structural components. Lamb waves have been used to study structures with a step discontinuity, as in the case of a solar cell bonded to a larger substrate [3, 4]. Lamb waves have also been widely used to detect bond line defects in adhesively bonded structures [5, 6]. Signal amplitude and energy can be meaningful tools for detection of material discontinuities or defects in ultrasonic NDE, as these can cause attenuation of the signal. Understanding the baseline damping in a pristine material is therefore necessary to understand attenuation as a damage indicator. It should be noted that there are multiple contributing factors to amplitude attenuation in Lamb waves, including geometric spreading of the wavefront, material damping, loss to adjacent media, and dispersion [7, 8].

Implementing damping in a finite element model serves to increase the accuracy in predicting the characteristics of waves propagating in the material (e.g. [9]) and to have appropriate sensor density when scanning a large area (e.g. [7]). Lamb wave attenuation is often implemented in a problem as a complex stiffness matrix where the imaginary components represent the frequency dependent damping (e.g. [7, 9]). However, many finite element software do not have the option to input a complex stiffness matrix. Another way that damping can be introduced is Rayleigh damping (e.g. [10–12]).

In this paper, the material properties of an Ultem1000 plate, including stiffness proportional Rayleigh damping coefficients β are found experimentally and implemented into a finite element model of a solar cell assembly. A 2D representation is modeled in Abaqus/Explicit based on the work done by Green et al, using Ultem1000 as the substrate material, polycrystalline silicon as the cell material, and RTV566 as the adhesive [13]. Disbonds of varying lengths are created at the adhesive-substrate interface at both the edge and center of the bond line. Each case is solved with and without damping included and the results are compared. The aim of this study is to observe the effects of material damping on the propagation of simulated Lamb waves in a finite element model. The results are intended to inform future experiment design for in-space testing applications but can also be applied to other viscoelastic, multi-layer media.

MODEL AND DAMAGE ASSESSMENT

Numerical Models

A 2D model of an Ultem1000 plate is created in Abaqus/Explicit using experimentally determined material properties, with and without damping included. The model's linear and quadratic bulk viscosity parameters, which are default values set in Abaqus to suppress ringing and improve the modeling of high-speed dynamic events in the explicit solver, are set to 0 in order to compare the model to the experimental data [14]. Two point loads with 155 kHz 5-cycle Hann-windowed amplitude profiles are applied symmetrically on the top and bottom left corners of the plate. The left edge of the plate is assigned a symmetry boundary condition, and the bottom right corner is pinned. 200 μm CPE4R 2D plane strain elements are used for the mesh, sized to allow for a sufficient

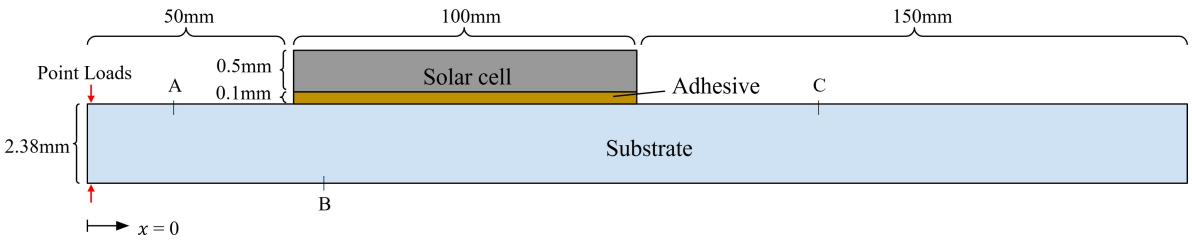

Figure 1. Diagram of the model used in simulation showing sensor locations A, B, and C

number of elements per wavelength and through the thickness of the plate. The time increment is set to 10 ns, which satisfies the CFL criterion [15]. Vertical displacements are collected at 6 sensors spaced in 25.4 mm (1 in) increments away from the source. Then, the peak amplitude at each sensor is normalized by the peak amplitude at the sensor nearest to the source. The normalized amplitude decay in the damped and undamped models is then compared to the experimental amplitude decay.

Next, a 2D model of the full solar cell assembly is created based on the specifications described in [13], Fig. 1 shows a diagram of the details. The same model parameters as described above are applied, including loading and boundary conditions. The mesh is set to 75 μm and locally refined to 33 μm through the thickness of the adhesive and 50 μm through the thickness of the solar cell. The time increment is set to 5 ns. Disbonds at the adhesive-substrate interface at both the left edge and center of the bond line, with sizes ranging 0 - 50 mm, are implemented with and without damping in the model. In the undamped cases, no damping is applied to any of the materials. In the damped cases, the same stiffness proportional damping constant is applied to both the adhesive layer and the substrate. The reasoning for this is that damping properties of silicone adhesives are not readily available, and at high frequencies, the material may behave reasonably similarly to Ultem1000.

Damage Indices

For the solar cell assembly model, vertical displacement signals are collected at sensor locations A, B, and C, (located at 20, 60, and 200 mm respectively) and are analyzed using a set of damage indices defined in [13]. Those yielding meaningful results are: taking the cross-correlation of the normalized damage signals with the normalized pristine signal at zero lag and dividing by the autocorrelation of the pristine signal with itself at zero lag (DI_1).

$$\mathrm{DI}_1 = \left| 1 - \frac{\mathrm{xcorr}_{\mathrm{def,pris}}\,|_{lag=0}}{\mathrm{autocorr}_{\mathrm{pris}}\,|_{lag=0}} \right|$$

And taking the difference between the normalized damage signal and the normalized pristine signal and summing over the result (DI_2).

$$\mathrm{DI}_2 = \frac{1}{N} \sum_{t \in \mathrm{t_{sim}}} A(t)$$

where $A(t)$ is the amplitude of the residual signal, $\mathrm{t_{sim}}$ is the simulation time and N is the number of samples in the signal.

EXPERIMENTAL MATERIAL CHARACTERIZATION

Experimental Setup and Dispersion Analysis

To determine the experimental material properties of the substrate, a 304 x 304 x 2.38 mm Ultem1000 plate is selected. Digital wave B225 broadband transducers are arranged on the plate in a pitch-catch configuration with one transducer acting as the source, and the other as the receiver. Measurements are taken at multiple frequencies between 50-200 kHz, at distances 1-6 in (25.4-152.4 mm) from the source. Data collection is repeated along three directions. A diagram of the experimental setup is seen in Fig. 2 (left).

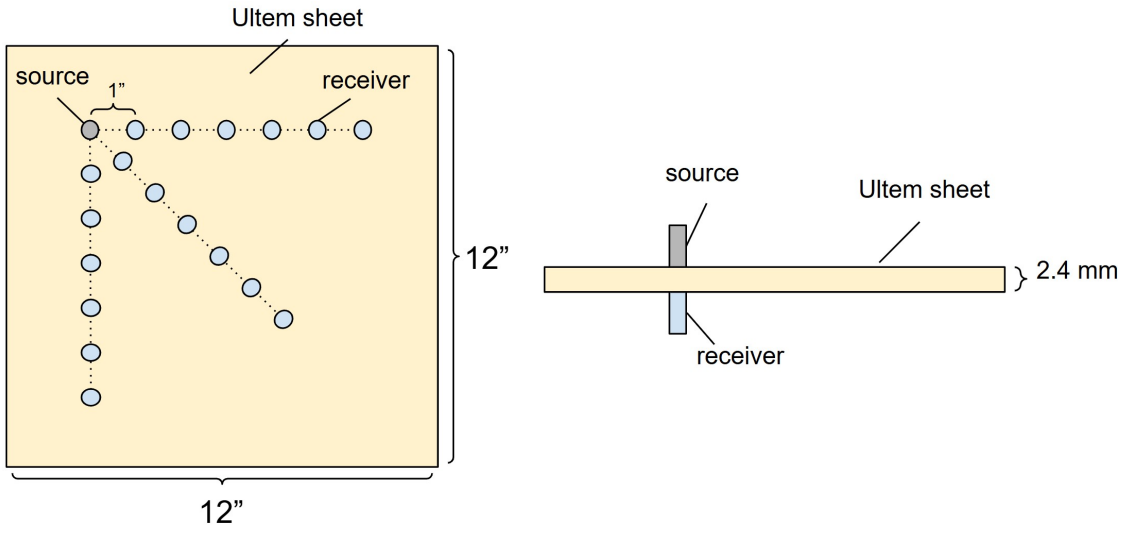

Figure 2. Experimental setup for obtaining Lamb wave damping (left) and shear wave velocity (right).

The shear wave velocity c_2 of the material is also measured experimentally by placing two Ultran SC25-5 shear transducers across the thickness of the Ultem plate as seen in Fig. 2 (right). The measurement is repeated at three different locations around the plate at 4-5 MHz. In order to calculate the shear wave velocity from the experimental signals, face-to-face reference measurements are taken [16]. Then, the reference time is subtracted from the total time of flight across the Ultem plate, and divided by the thickness, which is found with a micrometer at each measurement location.

Material damping

Lamb wave amplitude attenuation in an undamaged, homogeneous material is due to four main factors: (i) Geometric spreading, which is the amplitude loss due to increasing circular wavefront size with increasing distance from the source. (ii) Material damping, which is the loss due to imperfect elasticity in the material [7]. They are defined by:

$$A = A_0 \cdot \underbrace{\sqrt{r_0/r}}_{\text{geometric spreading}} \cdot \underbrace{e^{-k_i \Delta x}}_{\text{material damping}} \tag{1}$$

where A_0 is the initial amplitude at r_0, $\Delta x = r - r_0$, and k_i is the imaginary wavenumber. (iii) Dissipation into adjacent media, which can be ignored if the adjacent material is air. (iv) Wave dispersion, which is the loss due to the dispersive nature of Lamb waves.

It is desirable to have an easy and reliably accurate way to implement material damping in the numerical model. Therefore, Rayleigh damping is chosen due to simplicity and low computational cost [11]. In order to make use of Rayleigh coefficients for Lamb wave damping, wave propagation is equated with high frequency vibration, and Lamb wave amplitude decay is equated with vibration attenuation [10]. The relationship between the damping coefficient and the Rayleigh proportionality constants is given by:

$$c = \alpha m + \beta k \,, \tag{2}$$

where α is the mass proportional damping constant and β is the stiffness proportional damping constant. The relationship between the damping coefficient and the damping ratio is given by:

$$\zeta = \frac{c}{c_c} = \frac{1}{2}\left(\frac{\alpha}{\omega} + \beta\omega\right) \,, \tag{3}$$

where c_c is the critical damping coefficient and ω is the circular frequency. The logarithmic decrement of a wave with damping ratio ζ is:

$$\ln\left(\frac{u}{u_n}\right) = \frac{2\pi\zeta n}{\sqrt{1-\zeta^2}} \approx 2\pi\zeta n \,, \tag{4}$$

where u is the initial amplitude, u_n is the amplitude after n cycles, and $\zeta^2 << 1$ is assumed [17]. At high frequency, global vibration can be equated to local wave propagation. Thus, for a propagating Lamb mode with amplitudes A_1 and A_2 at an arbitrary distance Δx apart, Eq. (4) becomes an equivalent logarithmic decrement:

$$\ln\left(\frac{u}{u_n}\right) = 2\pi\zeta n = \ln\left(\frac{A_1}{A_2}\right) = k_i \Delta x \,. \tag{5}$$

This can be used to calculate the damping ratio by setting Δx = λ, the experimentally determined wavelength of the propagating Lamb wave at a given frequency, and n = 1:

$$\zeta = \frac{k_i \lambda}{2\pi} \,. \tag{6}$$

RESULTS AND DISCUSSION

The results of both experiments are combined to yield experimentally derived dispersion curves for Ultem1000. It is given that shear wave velocity c_2 is a function of material properties E, and ν, and density ρ. Then, using the experimental value for c_2, a range of possible (E, ν) combinations are input into DispersionCalculator [18]. The group velocities from the first part of the experiment are then compared to the predicted curves and the best match is found to be $E = 3.653$ GPa, and $\nu = 0.25$. The dispersion curve and the group velocity data can be seen in Fig. 3 (left).

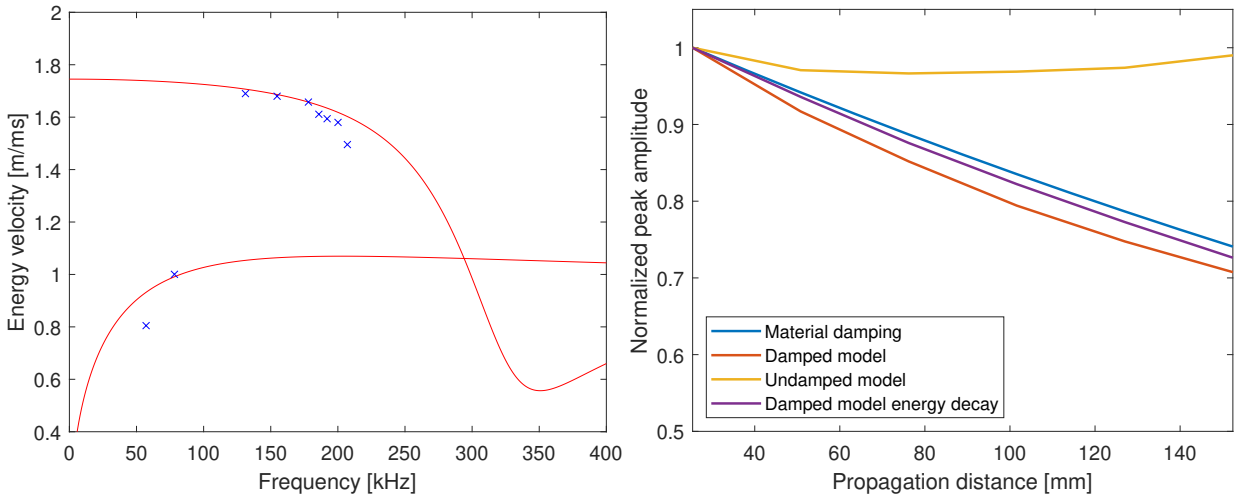

Figure 3. Experimental group velocity dispersion curve for a 2.38 mm thick Ultem1000 plate (left) and the experimental material damping compared to damped and undamped finite element model results (right).

The experimental Rayleigh constants β are determined by plugging Eq. (6) into Eq. (3), and assuming α = 0, since Rayleigh damping is dominated by stiffness proportional damping at higher frequencies, yielding:

$$\beta = \frac{k_i \lambda}{2\pi^2 f} \,. \tag{7}$$

For $f = 155$ kHz (center frequency), β is found to be 8.61e-9 s/rad, which is applied as the damping constant of the substrate and adhesive layers in the numerical model.

Using this damping constant and the material properties given in Table I, the simulated amplitude decay in the 2D model of the Ultem plate can be compared to the experimental data. Figure 3 (right) shows the normalized amplitude decay in both a damped and undamped model as well as the exponential decay fit curve of the experimental material damping data as derived from Eq. (1). The figure shows that the undamped 2D model does not capture amplitude decay, only some phase change and minor dispersion or numerical losses. The damped model, however, is able to capture the attenuation seen in the experimental data. The normalized wave packet energy of the damped signals is also plotted in the figure. The wave packet energy is found by summing the squared amplitude of a signal over the time window containing the main packet [11]. It aligns more closely with the experimental as it is less affected by dispersion and phase shift.

Implementing the experimental material properties into the solar cell assembly model, the results of applying DI_1 to the signals collected at sensor C, located after the cell, are seen in Fig. 4 (left). There is a clear linear trend of increasing damage index value with

TABLE I. Material properties used in the finite element model

Material	Young's modulus E (GPa)	Poisson's ratio ν	Density ρ (kg/m^3)	Rayleigh constant β (s/rad)
Polycrystalline silicon	160	0.28	2330	0
RTV566 [19]	0.00345	0.45	1490	8.61e-9
Ultem1000	3.653	0.25	1279.5	8.61e-9

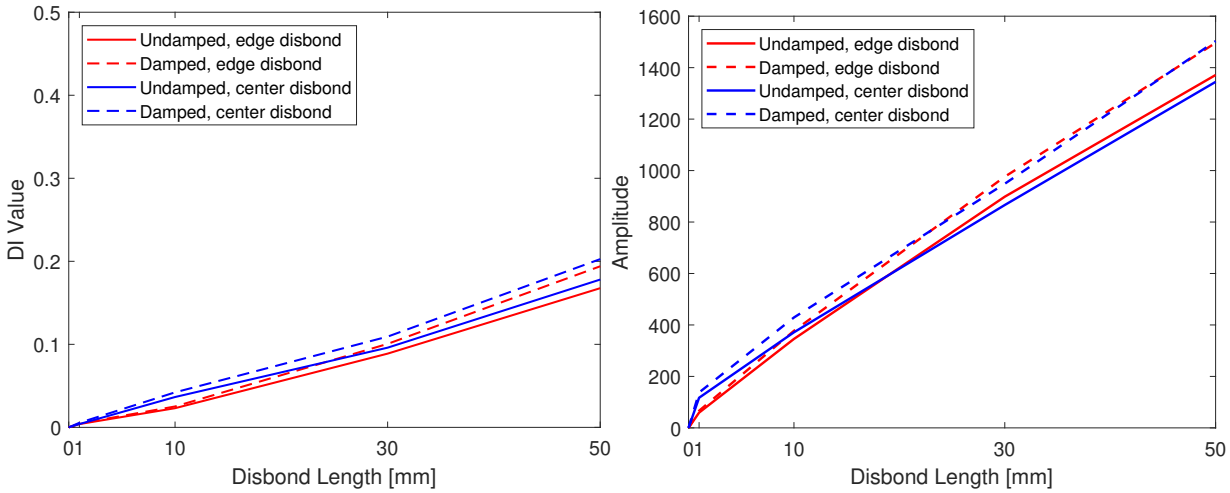

Figure 4. DI 1 (left) and DI 2 (right) values vs disbond size for centered and edge disbonds calculated from readings at sensor C.

increasing disbond size for both edge and centered disbonds, and the values are similar for both damage locations. This indicates that DI_1 could be used to characterize defects by size but not location. Adding damping to the model leads to slightly increased DI_1 values. The results of applying DI_2 to the signals collected at sensor C, located after the cell, are seen in Fig. 4 (right). These also show a linear trend and an increase in value with damping, indicating a similar usefulness in detecting and sizing disbonds.

Thus, a model without damping implemented could lead to overestimating a disbond size. It should also be noted that all the values presented here are those calculated at sensor C since they proved to be more useful than those calculated from the other sensor locations. In other words, a sensor located after the cell provides more reliable damage characterization for the given model and damage indices.

CONCLUDING REMARKS

Experimental material properties (E, ν) and Rayleigh damping coefficients β are obtained for Ultem1000. They are then applied to a finite element model of a solar cell assembly in which Ultem1000 is the substrate material. Results are compared between damped and undamped models with varying sized defects implemented at the bond line. It is seen that adding damping to the model increases the damage index value for the damage indices presented. This implies that using an undamped model could lead to over-predicting defect size. Future work may include obtaining experimental data for a full solar cell assembly or a representative laminate, as well as exploring the effect of adhesive properties on defect detection.

REFERENCES

1. Chakrapani, S. K., M. J. Padiyar, and K. Balasubramaniam. 2012. “Crack detection in full size Cz-silicon wafers using lamb wave air coupled ultrasonic testing (LAC-UT),” *Journal*

of Nondestructive Evaluation, 31:46–55.
2. Li, Y., C. He, Y. Lyu, G. Song, and B. Wu. 2019. "Crack detection in monocrystalline silicon solar cells using air-coupled ultrasonic lamb waves," *NDT & E International*, 102:129–136.
3. Chang, Z., D. Guo, and A. K. Mal. 1996. "Lamb wave propagation across a lap joint," *Review of Progress in Quantitative Nondestructive Evaluation: Volume 15A*:185–192.
4. Schaal, C. and A. Mal. 2016. "Lamb wave propagation in a plate with step discontinuities," *Wave Motion*, 66:177–189.
5. Ramalho, G. M., A. M. Lopes, and L. F. da Silva. 2022. "Structural health monitoring of adhesive joints using Lamb waves: A review," *Structural Control and Health Monitoring*, 29(1):e2849.
6. Masserey, B., C. Raemy, and P. Fromme. 2014. "High-frequency guided ultrasonic waves for hidden defect detection in multi-layered aircraft structures," *Ultrasonics*, 54(7):1720–1728.
7. Schubert, K. J. and A. S. Herrmann. 2011. "On attenuation and measurement of Lamb waves in viscoelastic composites," *Composite Structures*, 94(1):177–185.
8. Pollock, A. A. 1986. "Classical wave theory in practical AE testing," *Progress in acoustic emission III-JAP society of non-destructive testing*:708–721.
9. Mal, A. K., Y. Bar-Cohen, and S.-S. Lih. 1992. "Wave attenuation in fiber-reinforced composites," in *M 3 D: Mechanics and Mechanisms of Material Damping*, ASTM International.
10. Ramadas, C., K. Balasubramaniam, A. Hood, M. Joshi, and C. Krishnamurthy. 2011. "Modelling of attenuation of Lamb waves using Rayleigh damping: Numerical and experimental studies," *Composite Structures*, 93(8):2020–2025.
11. Gresil, M. and V. Giurgiutiu. 2015. "Prediction of attenuated guided waves propagation in carbon fiber composites using Rayleigh damping model," *Journal of Intelligent Material Systems and Structures*, 26(16):2151–2169.
12. Mardanshahi, A., M. Shokrieh, and S. Kazemirad. 2022. "Simulated Lamb wave propagation method for nondestructive monitoring of matrix cracking in laminated composites," *Structural Health Monitoring*, 21(2):695–709.
13. Green, M., F. Alsaffar, A. Mal, and C. Schaal. 2024. "Lamb Wave-Based Inspection of Solar Cell Arrays," in *ASME International Mechanical Engineering Congress and Exposition*, American Society of Mechanical Engineers, vol. 88612, p. V003T05A013.
14. Systemes, D., "Getting Started with ABAQUS/Explicit: Keywords Version," Section 3.6.1 Bulk viscosity.
15. Courant, R., K. Friedrichs, and H. Lewy. 1967. "On the partial difference equations of mathematical physics," *IBM journal of Research and Development*, 11(2):215–234.
16. Shih, J.-H., A. Mal, and M. Vemuri. 1998. "Plate wave characterization of stiffness degradation in composites during fatigue," *Research in nondestructive evaluation*, 10:147–162.
17. Meirovitch, L. 2010. *Fundamentals of vibrations*, Waveland Press.
18. Huber, A. 2018, "Dispersion Calculator," .
19. Salama, M., W. Rowe, and R. Yasui. 1973. "Thermoelastic analysis of solar cell arrays and their material properties," Tech. rep., NASA JPL.